EXPERIMENTAL AND NUMERICAL INVESTIGATION OF HYSTERESIS IN MULTIPHASE FLOW IN A MICROCHANNEL

Eugen Chiriac[1], Marioara Avram[2], Corneliu Bălan[3]

The paper is concerned with the experimental and numerical investigations of the hysteresis effect of an interface between two immiscible liquids in a microfluidic Hele-Shaw configuration. The two fluid samples are mineral oil and isopropyl alcohol, characterized by a small interfacial tension, low densities, and high viscosity ratio. The microfluidic test bifurcation has 3 branches connected in one channel. The viscous oil thread surrounded by alcohol is formed in the center of the geometry, immediately after junction. The hysteresis of the thread's width is analyzed at symmetric imposed cycles of input pressure for the mineral oil, the alcohol flow rate on the side branches being maintained constant. The gravity influence on the hysteresis curves is investigated using the direct visualization of the interface corroborated by the 3D numerical simulations performed with the VoF method implemented in ANSYS Fluent code.

Keywords: microfluidics, interface, multiphase flow, CFD
MSC2020: 76-05, 76M12, 76T06.

1. Introduction

Even though hysteresis is a phenomenon specific to magnetism and electricity it has been previously reported in fluids [1], [2], [3]. In [4] was shown that multiphase flow in a microfluidic T-junction exhibits hysteresis. Different flowing regimes, flow patterns were investigated alongside a decrease of the interfacial tension between the working fluids. The decrease of the interfacial tension had a high influence on the width of the hysteresis cycle. In [5], foam hysteretic behavior was investigated using a microfluidic device. An increase of viscosity generated the lag effect and it was enhanced by an increase of the surface tension. The importance of this phenomenon derives from the fact that many applications can be affected by it. As an example, when the flowing regimes are tested in a microchannel, the experiments are extended on a long period of time and the microchannel is subjected to a

[1] PhD. Student, REOROM Lab., University POLITEHNICA of Bucharest, Romania, Scientific Researcher, Lab. of Micro- Nano- Fluids, National Institute for R&D in Microtechnologies - IMT Bucharest, e-mail: eugen.chiriac@upb.ro

[2] Scientific Researcher I, National Institute for R&D in Microtechnologies - IMT Bucharest, Lab. of Micro- Nano- Fluids, e-mail: marioara.avram@imt.ro

[3] Professor, REOROM Lab., University POLITEHNICA of Bucharest, Romania, e-mail: corneliu.balan@upb.ro

hysteresis behaviour. In this paper we investigated, by experiments and numerical means, the hysteresis phenomenon in multiphase flow in a microchannel by using two immiscible liquids with low interfacial tension between them, mineral oil and isopropyl alcohol. We assessed as well the influence of gravity on the hysteresis cycle and on the flow field.

2. Methods and materials

The design of the microfluidic device is represented by a microchannel with three inlets, a junction and an outlet. Before and after the junction the channel has a length of $20mm$. The angle between the central branch and the side branches before the junction is of 30°. The microchannel has a depth of $50\mu m$, and a low aspect ratio (depth / width = 0.125). Based on this design, two microfluidic devices were fabricated, one in silicon, and the other one in PDMS (polydimethylsiloxane).

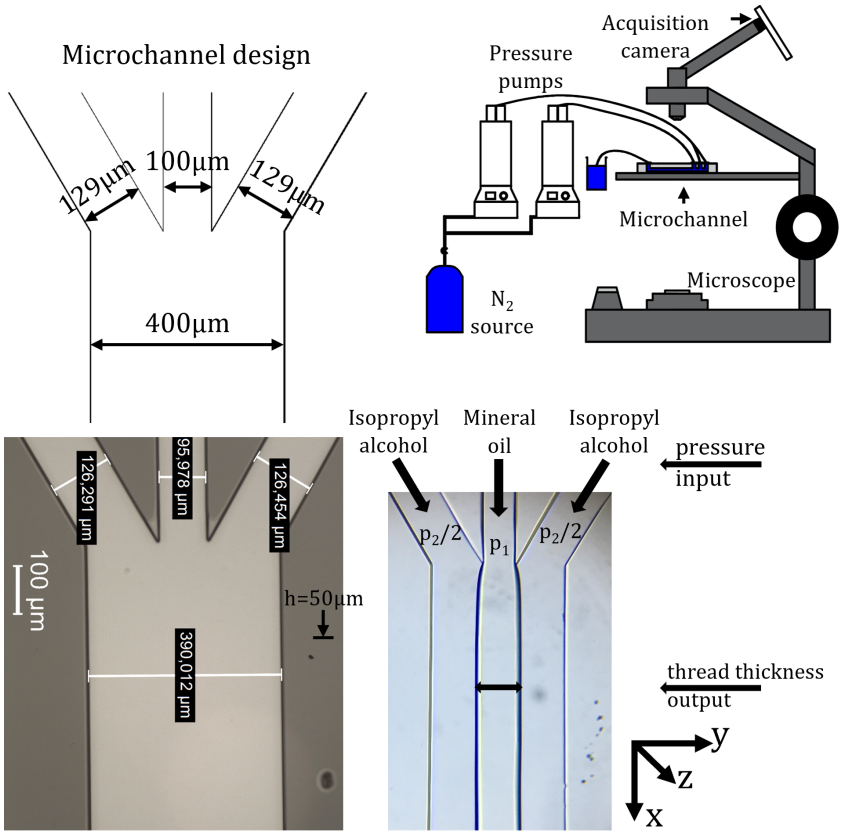

FIGURE 1. Microchannel design, schematic of the experimental setup, characteristic dimensions of PDMS microchannel, and hysteresis setup.

The one in silicon was done by etching of a silicon wafer using a Bosch process, and sealed with a 3 mm thick PDMS layer. On top of the PDMS seal, a glass slide was attached

to protect the PDMS sealing from dust and fingerprints, thus resulting in a microchannel with three rigid surfaces (bottom and sidewalls) and a slightly elastic top surface.

The second microchannel was fabricated in PDMS using soft lithography. The PDMS microchannel peeled from the silicon mold is sealed with a flat PDMS substrate. The complete procedure of microfabrication is described in [6].This type of channel has all the interior walls made of PDMS. This is important as PDMS is not a rigid material, even though high thickness PDMS films reach a certain level of rigidity, the surfaces are still elastic allowing a small degree of expansion and contraction depending on flow parameters. In both cases, there is a discrepancy between the designed dimensions and the actual widths of the fabricated microchannels mostly due to the UV exposure and development steps used during the patterning of the photoresist layer, which were not accurately optimized. A practical difference between the two devices is that different microscopes have to be used to perform the study, since visible light cannot pass through a silicon wafer.

The experimental setup is composed of two microscopes, a regular one and an inverted one, pressure pumps and image acquisition system and a schematic of it is presented in Fig. 1. The PDMS microchannel can be used with both microscopes while the silicon microchannel can only be used with the inverted microscope. The fluids used were a mineral oil with high viscosity and isopropyl alcohol due to the low interfacial tension between them [7]. Their material properties at $25°C$ are presented in Table 1.

TABLE 1. Material properties of working fluids at $25°C$.

Sample	$\rho[kg/m^3]$	$\eta[mPa \cdot s]$	$\sigma[mN/m]$
Isopropyl Alcohol	786	2.4	1.2
Mineral Oil	873	160	

3. **Experimental details**

A phenomenon was observed when multiphase flow experiments were performed in the trifurcation microchannel using mineral oil and isopropyl alcohol (IPA). The IPA was used as a continuous phase on the side branches of the microchannel while the mineral oil was used as a dispersed phase on the central branch. The confinement of the geometry allows flow stabilization [8], without any instabilities occurring, but the low aspect ratio of the microchannel contributes to the flow stabilization, by having a Hele-Shaw type channel [9]. This phenomenon takes place when, from the initial pair of pressure at the inlets of the microchannel, the pressure on the sides is kept constant and the pressure on the central branch of the channel is varied, such as, a different thread width is obtained at the same pair of pressures. For the hysteresis cycle, the input is the pressure and the output is the thread thickness, as it can be seen in Fig. 1 right. In fact, when returning the initial set

of pressures, the thread width was lower than the thread width from the beginning of the experiment for the PDMS microchannel.

To test this experiment in a controlled manner, at first the base pressure was investigated in order to always have the same flowing regime when returning to initial state, as such the pressure for the continuous phase (IPA) was found $p_2 = 600mbar$. By using a splitter, a pressure of $300mbar$ was ensured on each side of the microchannel. This pressure translates into a velocity of $0.0984m/s$ and a *Reynolds* number of 2.32. So, the flow on the side branches of the microchannel is inertial.

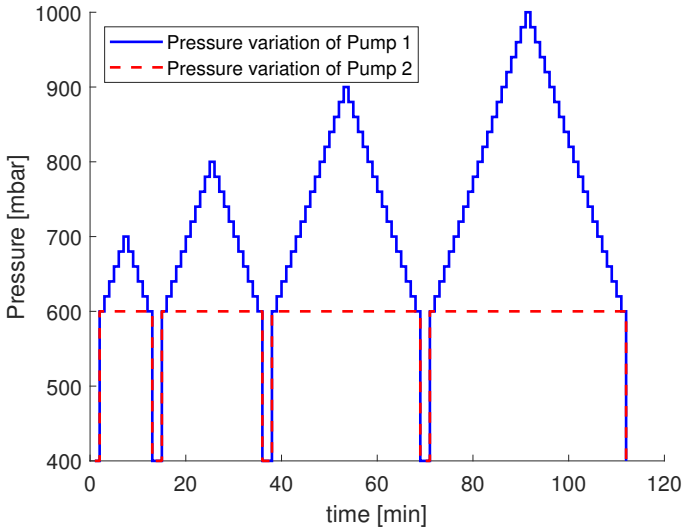

FIGURE 2. Inlet Pressure variation with time: Pump 1 - oil phase, Pump 2 - IPA phase.

On the central branch of the microchannel the dispersed phase is the mineral oil. The pressure on the central branch of the microchannel, p_1, is varied in four stages by $20mbar$: i) from 600 to 700 $mbar$; ii) 600 to 800 $mbar$; iii) 600 to 900 $mbar$ and iv) 600 to 1000 $mbar$. To ensure that the experiments are performed in the same manner, after each subsequent stage, the pressure on both pumps is dropped to $400mbar$ for one minute and then increased to initial flow state: $p_1 = p_2 = 600mbar$. In Fig 2 the four stages are presented. All the time steps of the phases are equal to 1 minute. It was observed experimentally that after one minute the interface position is not changed drastically. Besides the horizontal experiments, the PDMS microchannel was turned vertical to check the influence of gravity.

4. **Results and discussion**

To evaluate the magnitude of this hysteresis cycle, the thread width was measured in MATLAB, at the same point in the geometry, further than $500\mu m$ away from the junction. The thread thickness was plotted against the pressure, and it was observed in Fig. 3 and Fig.

4 that in all the cases, when the pressure was decreasing from the maximum pressure allowed for each stage, the thread width was smaller than the one obtained when the pressure was increasing for the PDMS microchannel. Furthermore, when the channel was turned vertical, when the gravity was no longer acting on z-axis but on y-axis and a change was observed in the system. The area of the hysteresis cycle was reduced in all the cases and at this point the influence of gravity at microscale cannot be neglected.

To evaluate the magnitude of this hysteresis cycle, the thread width was measured in MATLAB, at the same point in the geometry, further than $500\mu m$ away from the junction. The thread thickness was plotted against the pressure, and it was observed in Fig. 3 and Fig. 4 that in all the cases, when the pressure was decreasing from the maximum pressure allowed for each stage, the thread width was smaller than the one obtained when the pressure was increasing for the PDMS microchannel. However, for the silicon microchannel the process is reversed. When the pressure is decreasing, and the final state is reached, $p_1 = p_2 = 600mbar$, the thread has a higher thickness than the one from the initial state, and as the experiment continues, the thread thickness of the final state becomes the initial state for the next stage.

Furthermore, when the channel was turned vertical, when the gravity was no longer acting on the z-axis but on the x-axis a change was observed in the system. The area of the hysteresis cycle was reduced in all the cases and at this point the influence of gravity at microscale cannot be neglected.

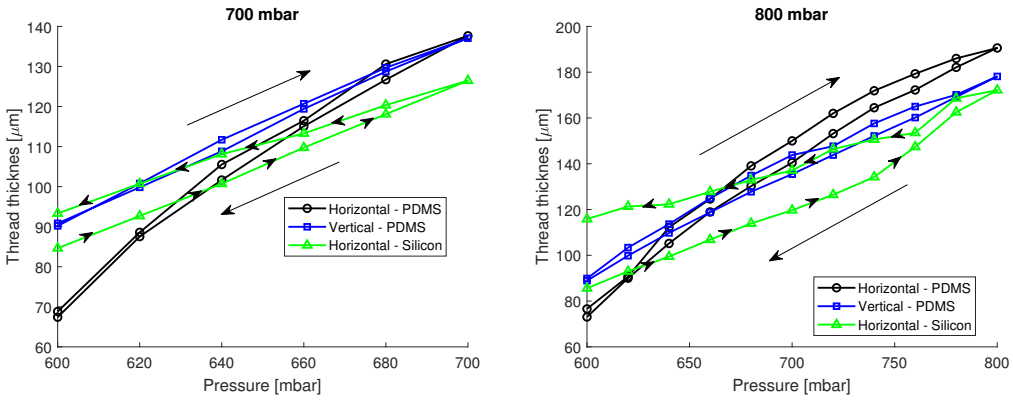

FIGURE 3. Hysteresis cycle stage I. 600 – $700mbar$ & II. 600 - $800mbar$.

In Fig. 3 and Fig. 4 the three hysteresis cycles are compared for the four stages, when the maximum pressure is 700, 800, 900 and 1000 $mbar$. In all cases the influence of gravity is observed. There is a small difference between the initial thickness of the thread when $p_1 = p_2 = 600mbar$. This difference is always present, especially when going from experiment to experiment. As an example, during the experiments, when the four stages are performed continuously, the experiments take place for two hours. During this time, when returning from the maximum pressure to the minimum pressure, the thickness of the thread

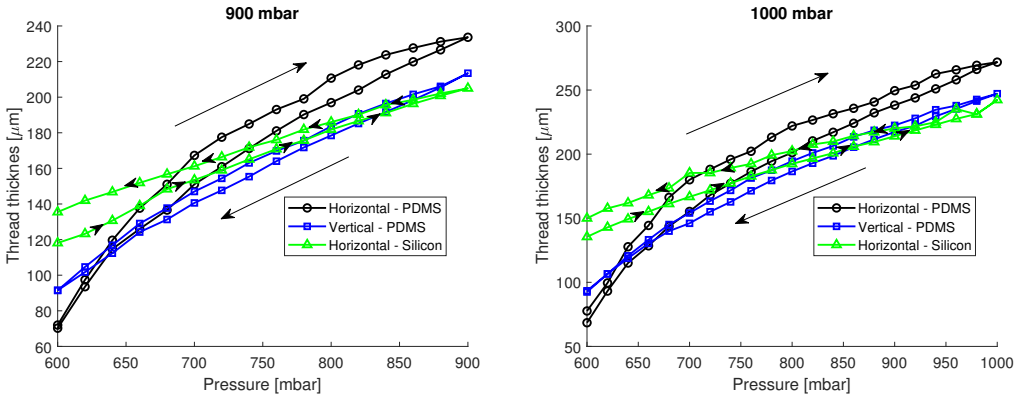

FIGURE 4. Hysteresis cycle stage III. 600 – 900$mbar$ & IV. 600 - 1000$mbar$.

is increased by a small margin (a few micrometers), the more used is the microchannel the more will the thread thickness increase for the next subsequent stage.

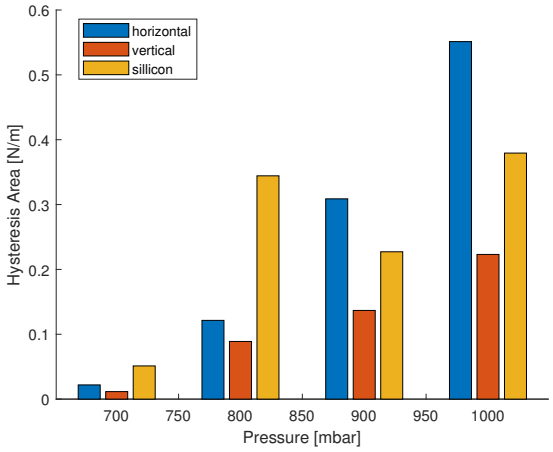

FIGURE 5. Comparison of the area of the hysteresis cycle when the microchannel is microfabricated from PDMS and silicon.

The area of the hysteresis cycle was investigated for all stages and it is presented in Fig. 5. For the first two stages the area obtained for the silicon microchannel is much higher than the area obtained for the PDMS microchannel. The material properties play an important role here. PDMS is an elastic material that deforms at high pressure. In this case, it attenuates the pressure change in the system. Opposed to it is the silicon, which is a rigid material, and it transfers the pressure change directly into the microchannel. In all the cases, the hysteresis area for the horizontal microchannel is higher than the area obtained for the vertical channel, so gravity reduces the hysteresis area that is the dissipated energy of the system.

5. Numerical Simulations of the interface

Two 3D numerical simulations are performed with the initial flow state: $p_1 = p_2 = 600mbar$ but with the direction of gravity changed, to obtain further insights from the flow. To solve the multiphase flow, the Fluent code from ANSYS is used with the Volume of Fluid method. Three equations are solved numerically, mass conservation, momentum conservation - one equation for both phases, where the material properties are averaged with the phase fraction [10], and a transport equation that tracks the interface. Taking into account that the fluids are Newtonian, incompressible and immiscible, the equations take the following form:

$$\nabla \cdot \mathbf{v} = 0, \tag{1}$$

$$\rho \left(\frac{\partial v}{\partial t} + (\mathbf{v} \cdot \nabla) \mathbf{v} \right) = -\nabla p + \eta \nabla^2 \mathbf{v} + \rho \mathbf{f} + \mathbf{F_s}, \tag{2}$$

$$\frac{\partial \alpha}{\partial t} + \nabla \cdot (\alpha \mathbf{v}) = 0, \tag{3}$$

where $\mathbf{v}$ is the velocity vector, p is the pressure, $\mathbf{f}$ is the gravity, ρ is the averaged density, η is the averaged viscosity and $\mathbf{F_s}$ is the surface tension force. The averaged material properties are computed using the volume fraction, α:

$$\rho = \alpha \rho_{IPA} + (1 - \alpha) \rho_{oil}, \tag{4}$$

$$\eta = \alpha \eta_{IPA} + (1 - \alpha) \eta_{oil}. \tag{5}$$

The source term added to the momentum equation is a volume force that takes into account the effects of the surface tension $\mathbf{F_s}$, and it is modeled using the Continuum Surface Force model [11], [12]. In the CSF model the source term is $\mathbf{F_s} = \sigma \kappa \nabla \alpha$ and in Fluent it takes the following form:

$$\mathbf{F_s} = \frac{2\rho}{\rho_{IPA} + \rho_{oil}} \sigma \kappa \nabla \alpha, \tag{6}$$

where σ is the interfacial tension, κ is the curvature, $\kappa = \nabla \cdot (\nabla \alpha / |\nabla \alpha|)$.

The domain consists of a shortened version of the microchannel, 5 mm before the junction, 1 cm after the junction, and it has a more refined zone junction zone. The mesh has approximately 1 million cells, 3 millions faces and 1 million nodes. In terms of quality, the minimum orthogonal quality is 0.5 and a maximum aspect ratio of 6.74. As the boundary conditions, the inlets are velocity inlets, the outlet is pressure outlet, and as initial condition $v_1 = v_3 = 0.09841 m/s$ for the alcohol phase, while for the oil phase $v_2 = 0.002675 m/s$.

The VOF formulation used for these simulation was implicit as it allows larger time steps. For the transient formulation the *Bounded Second Order Implicit* scheme was chosen while for the spatial discretization schemes the following were chosen: *Least Squares Cell*

Based for the Gradient, *PRESTO!* for Pressure, *Second Order Upwind* for Momentum and *Modified HRIC* for the Volume Fraction. The initial time step was set to $\Delta t = 10^{-5}s$ and by using an adaptive time step, with the condition of the Courant number being 1, the maximum allowed time step was $\Delta t = 2 \cdot 10^{-5}s$.

The only difference between the numerical simulations is the direction on which the gravity is acting, for the horizontal microchannel, the gravity is acting on the z axis, while for the vertical microchannel the gravity is acting on the x axis.

At first, a qualitative validation is done for both simulations in Fig. 6. The phase contours are compared with flow visualizations obtained in the same flow state. The results of the numerical simulations are in good agreement with the experimental visualizations, by capturing two key points, the curvature of the interface at junction and the thinning of the thread.

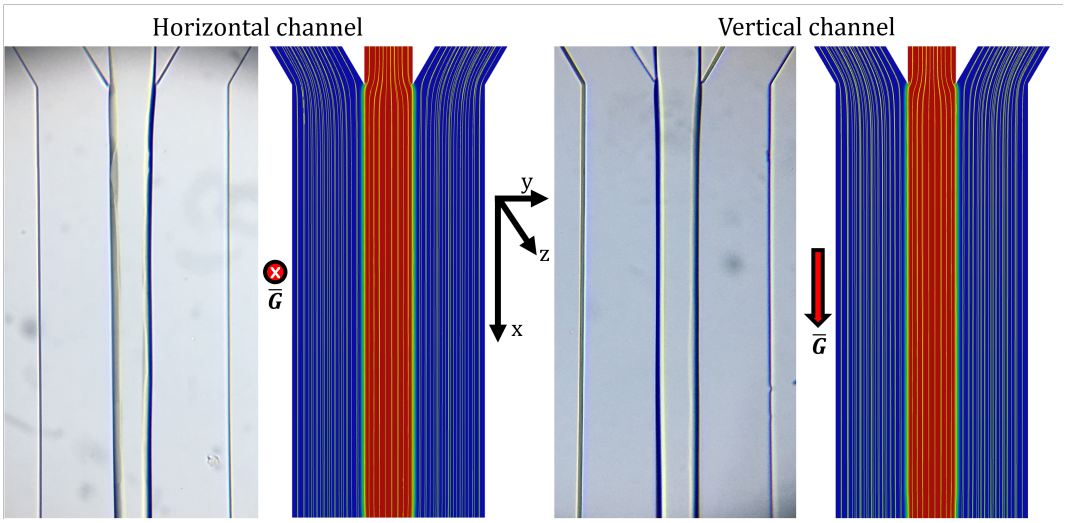

FIGURE 6. Qualitative validation of numerical simulations by using phase contours with pathlines against flow visualizations.

The two numerical simulations are compared one against each other at the same simulation time $t = 1s$. In Fig. 7 the velocity distributions are compared on a line perpendicular to the flow field, placed at 500 micrometers away from the junction and in the middle of the channel ($h = 25\mu m$). The two velocity distributions match each other. Next, the wall shear stress is analyzed on the right wall of the microchannel, after the junction, at $h = 25\mu m$. Again, the two distributions match each other.

The difference between the numerical simulations is obtained in terms of static pressure, in Fig. 8. The distributions of static pressure are displayed on six perpendicular lines perpendicular to the flow field, starting from the junction with a step of $100\mu m$. For both pressure distributions, pressure jumps are recorded at the interface, meaning that the interface is not straight and it has a curvature. The main difference comes in terms of static

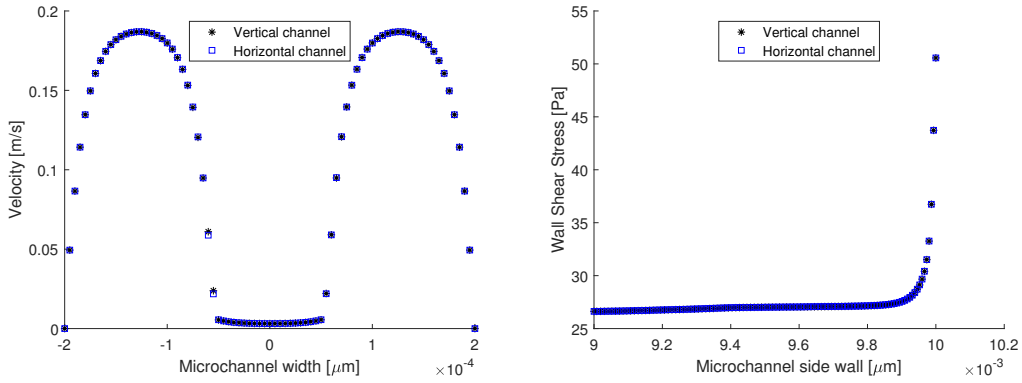

FIGURE 7. Velocity distribution on a line perpendicular to the flow field positioned at $500\mu m$ from junction and Wall Shear Stress variation on a side wall after the junction at $t = 1s$.

pressure magnitude, meaning that less pressure is required to flow for the microchannel that is placed vertically, as a difference of $\approx 40Pa$ is recorded between the two distributions.

6. **Conclusions**

To sum up the present findings, the presence of the hysteresis was highlighted in Fig. 3 and Fig. 4. The gravitational force plays an important role on the hysteresis cycle, its influence is highlighted in Fig. 5, where the area of the hysteresis was reduced when the gravitational force was acting on the flowing direction. 3D VoF numerical simulations were performed on the initial flow state and the influence of gravity was highlighted once again in Fig. 8, by having a difference in Static Pressure.

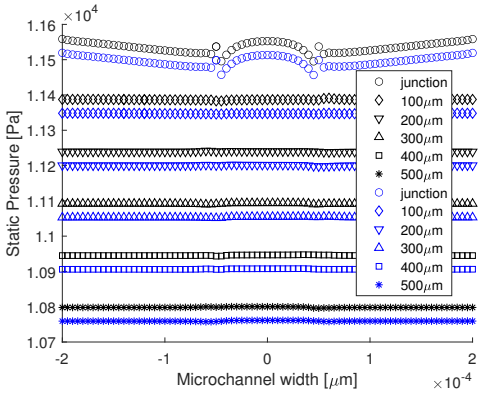

FIGURE 8. Distributions of static pressure on perpendicular lines to the flow field at $t = 1s$, black horizontal channel, blue vertical channel.

Acknowledgment

This work was supported by the grant of PN-III-P2-2.1-PED-2019-3514 (Project No.510 PED) and of CHIST-ERA -19 - XAI 009 MUCCA project, by the founding of EC and The Romania Executive Agency for Higher Education, Research, Development and Innovation Funding - UEFISCDI, grant COFUND-CHIST -ERA MUCCA no. 206/2019.

REFERENCES

[1] *Z. Shi, Y. Zhang, M. Liu, D. A. H. Hanour and Y. Gan*, Dynamic contact angle hysteresis in liquid bridges, Colloids and Surfaces A: Physicochemical and Engineering Aspects, **555** (2018).

[2] *L. Hai-Long, H. R. Liu and H. Ding*, A fully 3D simulation of fluid-structure interaction with dynamic wetting and contact angle hysteresis, Journal of Computational Physics, **420** (2020)

[3] *Y. Gao, K. Wu, Z. Chen, T. Zhou, J. Li, D. Feng, Y. Gao and W. Tian*, Effect of wetting hysteresis on fluid flow in shale oil reservoirs, Energy & Fuels, **35** (2021)

[4] *M. Zagnoni, J. Anderson and J. M. Cooper*, Hysteresis in multiphase microfluidics at a T-junction, Langmuir, **26** (2010).

[5] *L. Labarre and D. Vigolo*, Microfluidics approach to investigate foam hysteretic behaviour, Microfluidics and Nanofluidics, **23** (2019).

[6] *E. Chiriac, A.M. Bran, C. Voitincu and C. Balan*, Experimental validation of VOF method in microchannel flows, ATEE, (2021).

[7] *E. Chiriac, A. M. Bratu, M. Avram and C. Bălan*, Alcohol jets investigations in a microchannel in a viscous outer medium, EENVIRO, **664** (2021).

[8] *C. Patrascu and C. Balan*, The stabilizing effect of confinement on a liquid jet in a viscous outer fluid, U.P.B. Sci. Bull., Series A, **81** (2019).

[9] *I. Chakraborty, J. Ricouvier, P. Yazhgur, P. Tabeling, and A. M. Leshansky*, Droplet generation at Hele-Shaw microfluidic T-junction, Physics of Fluids, **31** (2019).

[10] ANSYS Fluent Theory Guide, (2020), R2.

[11] *J.U. Brackbill, K. B. Douglas and C. Zemach*, A continuum method for modeling surface tension, Journal of computational physics, **100** (1992).

[12] *S. Popinet*, Numerical models of surface tension, Annual Review of Fluid Mechanics, **50** (2018), 49-75